Topological Edge States and Gap Solitons in the Nonlinear Dirac Model

*Daria A. Smirnova, Lev A. Smirnov, Daniel Leykam, and Yuri S. Kivshar**

Topological photonics has emerged recently as a novel approach for realizing robust optical circuitry, and the study of nonlinear effects in topological photonics is expected to open the door for tunability of photonic structures with topological properties. Here, the topological edge states and topological gap solitons which reside in the same band gaps described by the nonlinear Dirac model are studied, in both one and two dimensions. Strong nonlinear interactions between these dissimilar topological modes, manifested in the efficient excitation of topological edge states by scattered traveling gap solitons are revealed. Nonlinear tunability of localized states is explicated with exact analytical solutions for the two-component spinor wave function. Our studies are complemented by spatiotemporal numerical modeling of the nonlinear scattering in 1D and 2D photonic lattices.

The grand vision of robust waveguiding and routing of light motivates studies of topological photonic systems.[1,2] Nonlinear effects are now pursued as a means of combining topological protection with functionalities such as active tunability, nonreciprocity, frequency conversion, and entangled particle generation.[3–12] For example, nonlinearity can control the propagation of topological edge states through self-focusing,[4,13–18] or even induce topological band gaps and unidirectional edge states in topologically trivial systems.[19–22] Theoretical studies of these phenomena so far have largely focused on i) generic continuum nonlinear Schrodinger equations in which nonlinearity compensates the linear edge state dispersion to form edge solitons,[15,17,23] and ii) numerical simulations of 2D nonlinear lattice models that remain quite challenging to implement in optics, requiring, for example, nonlinear coupling,[3,10,24–28] exciton–polaritons in strong external magnetic fields,[4,13,15–18] or longitudinally modulated waveguide arrays.[14,20,21]

Recently, 1D experiments using coupled optical fibre loops[29] have demonstrated coupling between bulk states and topological edge states mediated by local on-site Kerr nonlinearity. This opens a new degree of freedom for control over the topological edge states, as bulk band gaps prevent this coupling in static linear systems. The aim of this letter is to systematically study this phenomenon using a generic continuum model of topological photonic lattices, focusing on transformations between self-trapped gap solitons and topological edge states.

We study a nonlinear Dirac model with local Kerr nonlinearity describing bulk solitons and nonlinear edge states in a variety of 1D and 2D nonlinear systems, including the SSH, honeycomb, and kagome lattices, see, for example, **Figure 1**. This model supports exact analytic solutions for both the bulk gap and edge solitons, including their dispersion and envelope profiles, providing a convenient setting for analyzing interactions and scattering between the two. We find that the mid-gap frequency appears as a critical point at which the bulk gap soliton destabilizes and the topological edge state emerges. Numerical simulations reveal that scattering of travelling bulk solitons off the edge can excite the edge states with high efficiency (≈ 20%), and that there is an optimal soliton velocity maximizing the energy transfer. Perfect phase matching of this interaction is, however, inhibited by the aforementioned bulk soliton instability. Our model explicates nonlinear tunability and transport properties of spin-polarized localized nonlinear modes residing in topological band gaps and complements recent theoretical and experimental studies.[16,29,30]

We begin with the nonlinear Dirac model describing evolution of a spinor wavefunction $\Psi = [\Psi_1, \Psi_2]$

$$i\partial_t \Psi = (\hat{H}_D(\delta \boldsymbol{k}) + \hat{H}_{NL})\Psi \tag{1}$$

$$\hat{H}_D(\delta \boldsymbol{k}) = \delta k_x \hat{\sigma}_x + \delta k_y \hat{\sigma}_y + M\hat{\sigma}_z \tag{2}$$

where $\delta \boldsymbol{k} = (\delta k_x, \delta k_y) \equiv -i(\partial_x, \partial_y)$ is the momentum and $\hat{H}_{NL} = -g\left[|\Psi_1|^2, 0; 0, |\Psi_2|^2\right]$ is a local cubic nonlinearity. We reduce Equation (1) to a quasi-1D form by considering plane wave states along the x axis with wavenumber k, $\Psi = \psi e^{ikx}$,

$$i\partial_t \psi = \begin{pmatrix} M - g|\psi_1|^2 & k - \partial_y \\ k + \partial_y & -M - g|\psi_2|^2 \end{pmatrix} \psi \tag{3}$$

Dr. D. A. Smirnova, Prof. Y. S. Kivshar
Nonlinear Physics Centre
Australian National University
Canberra, ACT 2601, Australia
E-mail: ysk@internode.on.net
Dr. D. A. Smirnova, Dr. L. A. Smirnov
Institute of Applied Physics
Russian Academy of Science
Nizhny Novgorod 603950, Russia
Dr. D. Leykam
Center for Theoretical Physics of Complex Systems
Institute for Basic Science (IBS)
Daejeon 34126, Republic of Korea

The ORCID identification number(s) for the author(s) of this article can be found under https://doi.org/10.1002/lpor.201900223

DOI: 10.1002/lpor.201900223

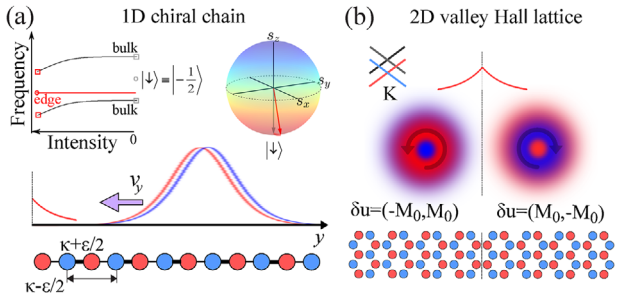

Figure 1. Applications of the nonlinear Dirac model. a) Gap soliton excites topological edge state of a 1D dimerized chain. Left inset: Schematic of the intensity-controlled tunability of the edge state frequency. Right inset: Bloch sphere representation of edge state spin polarization, tilted due to nonlinearity. b) Semi-vortex bulk solitons and edge states at a valley-Hall domain wall in graphene with staggered sublattice potential.

Conserved quantities are the power $\mathscr{P} = \langle\psi|\psi\rangle$ and the energy $\mathscr{E} = \langle\psi|(\hat{H}_D + \frac{1}{2}\hat{H}_{NL})|\psi\rangle$, where the inner products denote integration over y. We seek stationary states with time dependence $\approx \exp(-i\omega t)$ and velocity v by applying the Lorentz transformation

$$\tau = \gamma(t - vy), \quad \xi = \gamma(y - vt), \quad \gamma = 1/\sqrt{1-v^2} \tag{4}$$

Recasting the nonlinear eigenvalue problem as a Hamiltonian system governing the mode profiles (Supporting Information), *all* localized modes (edge or bulk) must have vanishing Hamiltonian, enabling a closed form solution

$$\psi_1^s(\xi) = \sqrt{\frac{\rho_s}{2}}\left(e^{-i\alpha_s} + \gamma(1+v)e^{i\alpha_s}\right)e^{i\beta_s} \tag{5a}$$

$$\psi_2^s(\xi) = -i\sqrt{\frac{\rho_s}{2}}\left(e^{-i\alpha_s} - \gamma(1+v)e^{i\alpha_s}\right)e^{i\beta_s} \tag{5b}$$

where ρ_s, α_s, and β_s are intensity, spin angle, and phase profiles, respectively, which take the form

$$\alpha_n(\xi) = \tan^{-1}\left[\frac{\Omega-\omega}{\sqrt{\Omega^2-\omega^2}}\tanh\left(\sqrt{\Omega^2-\omega^2}\,\xi\right)\right]$$

$$\alpha_s(\xi) = \alpha_n - \delta/2, \quad \rho_s(\xi) = \frac{2(\Omega\cos 2\alpha_n - \omega)}{\mathscr{B} + \mathscr{A}\cos^2 2\alpha_s}$$

$$\beta_s(\xi) = v\sqrt{\frac{\mathscr{B}}{\mathscr{A}+\mathscr{B}}}\tan^{-1}\left(\sqrt{\frac{\mathscr{B}}{\mathscr{A}+\mathscr{B}}}\tan 2\alpha_s\right) \tag{6}$$

with coefficients $\mathscr{A} = \gamma(1+v)g$, $\mathscr{B} = \gamma g/(1-v)$, $\Omega = \sqrt{k^2+M_0^2}$, $\delta = \tan^{-1}(\frac{k}{M_0})$, and $M = M_0 \geq 0$. The $v = 0$ limit returns spinor components of the chiral soliton[16]

$$\begin{pmatrix}\psi_1^s(y)\\ \psi_2^s(y)\end{pmatrix} = \sqrt{2\rho_s(y)}e^{-i\omega(\mathscr{P})t}\begin{pmatrix}\cos\alpha_s(y)\\ -\sin\alpha_s(y)\end{pmatrix} \tag{7}$$

where the frequency $\omega(\mathscr{P})$ implicitly depends on the total power. Remarkably, this exact solution describes both bulk and edge solitons, with the latter interpreted as part of a stationary bulk soliton bound to the edge distinguished by the boundary conditions.

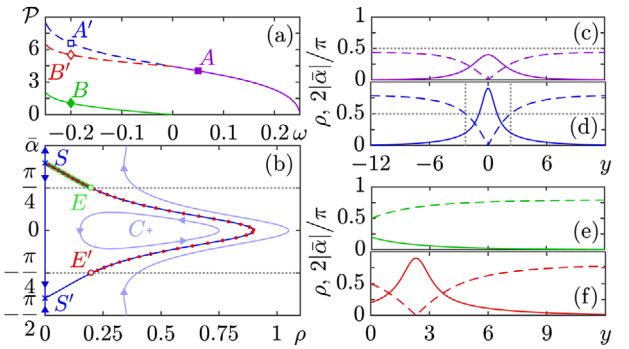

Figure 2. a) Nonlinear dispersion of stationary localized states: dependence of the frequency on the total power $\omega(\mathscr{P})$ for bulk solitons (violet solid for stable and dashed blue for unstable branches) and families of the edge states (solid green for stable localized at the half dimer and dashed red for unstable nonlinearly induced at the full dimer edge). b) Phase portrait of the nonlinear SSH model ($\omega = -0.075$) identify phase trajectories for soliton (blue) and edge states (green and red dotted). c,d) Stationary bulk solitons: profiles of c) stable and d) unstable solitons indicated by letters *A* and *A′* in panel (a). e,f) Nonlinear edge states: profiles for e) half-dimer (*B*) and f) full-dimer (*B′*) chain termination at the left edge. The intensity ρ is plotted with solid lines, dashed lines correspond to $2|\bar{\alpha}|/\pi$ (c–f). Parameters $v = 0$, $\kappa = 1$, $\nu_F = 1$, $g = 1$, $\varepsilon = 0.25$.

To exemplify features of these exact solutions, we consider the Su–Schrieffer–Heeger (SSH) model, describing a 1D dimer chain of single-mode cavities or waveguides with alternating weak and strong couplings $\kappa_{1,2} = \kappa \pm \varepsilon/2$ between nearest neighbors, see Figure 1a. The tight-binding equations governing the linear light propagation dynamics are

$$i\frac{d\Psi_n}{dt} + \left(\kappa - (-1)^n\frac{\varepsilon}{2}\right)\Psi_{n-1} + \left(\kappa + (-1)^n\frac{\varepsilon}{2}\right)\Psi_{n+1} = 0 \tag{8}$$

where Ψ_n is the field amplitude at the site n. Introducing two sublattices (even and odd elements), we recover the two-component form of Equation (8), see details in Section SIII, Supporting Information. Near the Brillouin zone edge $k_y d = \pi$ the bulk spectrum is captured by the continuum Dirac Hamiltonian given in momentum space by

$$\hat{H}_D(\delta k) = -\varepsilon\hat{\sigma}_x + v_F\hat{\sigma}_y\delta k \tag{9}$$

where $v_F = \kappa d$ is Fermi velocity and d is the lattice period. We assume the cavities form a Kerr nonlinear medium. Introducing on-site self-focusing nonlinearity, this corresponds to Equation (3) with $k = -\varepsilon$ and $M = 0$.

The phase plane $(\rho, \bar{\alpha})$ of the Hamiltonian system determining the mode profiles at $v = 0$ is shown in **Figure 2**b, where $\bar{\alpha} = \alpha_s - \pi/4$. There are three equilibrium points: two saddles $S, S'\rho = 0$, $\omega = \varepsilon\sin(2\alpha)$, and center C $\alpha = \pi/4$, $\rho = (\varepsilon - \omega)/g$. This phase portrait supports a bright soliton as a heteroclinic trajectory at vanishing Hamiltonian, corresponding to a separatrix between two saddles. In contrast to the nonlinear coupling model studied in refs. [25–27], the bounded trajectory here is unique. The boundary conditions i) $\alpha_s = \pi/2$ (half dimer edge) and ii) $\alpha_s = 0$ (full dimer edge) in Equation (7) describe linear edge states modified by nonlinearity and nonlinearity-induced edge states,

respectively. We verified these analytical solutions against stationary solutions found numerically using Newton's method.

Integrating the intensity of the soliton solutions Equation (1), we obtain their total power and energy

$$\mathscr{P}_s(\omega,\nu)=\frac{4}{g\gamma\sqrt{1+\gamma^2}}\left[\frac{\pi}{2}-\tan^{-1}\left(\frac{1}{\sqrt{1+\gamma^2}}\frac{\omega_s}{\sqrt{\varepsilon^2-\omega^2}}\right)\right] \quad (10a)$$

$$\mathscr{E}_s(\omega,\nu)=\omega_s(1-\gamma^2)\mathscr{P}_s+\frac{4\gamma^2\varepsilon}{g}\tan^{-1}\left(\frac{\sqrt{\varepsilon^2-\omega^2}}{\gamma\varepsilon}\right) \quad (10b)$$

where $\omega_s=\gamma\omega$ is the soliton frequency in the laboratory frame. In the linear limit $\omega\to\varepsilon$ the energy of nonlinear interaction vanishes and $\mathscr{E}_s\to\omega_s\mathscr{P}_s$. We similarly obtain the type (i) edge state dispersion

$$\mathscr{P}^{(1)}(\omega)=\frac{\sqrt{2}}{g}\tan^{-1}\frac{|\omega|}{\sqrt{2(\varepsilon^2-\omega^2)}} \quad (11)$$

with asymptotic values $\mathscr{P}^{(1)}(\omega\to 0)\to 0$ and $\mathscr{P}^{(1)}(\omega\to-\varepsilon)=\pi/g\sqrt{2}$. The power of the type (ii) edge state can then be calculated as the difference $\mathscr{P}^{(2)}=\mathscr{P}_s(\omega,\nu=0)-\mathscr{P}^{(1)}$ and has a nonzero threshold $\mathscr{P}^{(2)}(\omega\to 0)\to\sqrt{2}\pi/g$. The modal dispersion plotted in Figure 2a shows that the type (i) edge states bifurcate from the linear mid-gap topological edge modes at zero intensity, indicating the absence of any threshold necessary for their existence. They exist in the range $-\varepsilon<\omega(\mathscr{P})\le 0$ that can be controlled by dimerization strength ε. Notably, $\omega=0$ coincides with a bifurcation of the bulk soliton, which loses its stability and produces a type (ii) nonlinear edge state.

To relate these observations to the topological properties of the SSH model it is useful to study the soliton intensity and spin angle profiles (ρ,α), shown in Figures 2c–f. The latter determines the y-dependent spin polarization density $\boldsymbol{S}=\frac{1}{2}\psi^\dagger\hat{\sigma}\psi$. For solitons at rest, this yields $\boldsymbol{S}_s(y)=\rho_s(-\sin 2\alpha_s,0,\cos 2\alpha_s)$. The spin angle $\bar{\alpha}$ changes sign at the soliton core and localization requires $\bar{\alpha}$ to asymptotically approach $\cos 2\bar{\alpha}=\omega/\varepsilon$. The bulk solitons hence have total spin $\langle\boldsymbol{S}\rangle_s=\int\boldsymbol{S}\,dy=-2/g(\tan^{-1}(\sqrt{1-\omega^2\varepsilon^{-2}}),0,0)$, which respects the inversion symmetry of the bulk Hamiltonian. On the other hand, the edge solitons are obtained by asymmetrically cutting the bulk solitons into two pieces, such that they individually have nonzero S_z and break the sublattice inversion symmetry. This behavior is strongly reminiscent of the linear limit, in which topological edge states are created when the edge cuts a dimer in half.

Whether a dimer is cut by the edge is determined by the Zak phase Φ_B, which is quantized by inversion symmetry. When $\Phi_B=\pi$ (nontrivial phase) the Wannier centers lie at the cell boundary, corresponding to dimers cut by the edge. The Zak phase can be generalized to the nonlinear case by computing the nonlinear Berry phase of the delocalized modes comprising the bulk band structure.[31] For the nonlinear chain, provided the total dimer intensity $I\equiv|\psi_1|^2+|\psi_2|^2$ is lower than the critical value $I<2\varepsilon/g$, the bulk band structure features two dispersive pass bands, $\omega_\pm^{NL}(k_y)=\omega_\pm^L(k_y)-gI/2$, where linear dispersion $\omega_\pm^L(k_y)$ undergoes a uniform shift toward negative frequencies. The corresponding eigenfunctions $\mathbf{u}_\pm=\sqrt{\frac{I}{2}}(e^{-i\varphi(k_y)},\pm 1)$ do not change compared to the linear case, with the phase defined from relations $[\cos\varphi(k_y),\sin\varphi(k_y)]=\mathbf{h}/|\mathbf{h}|$, where $\mathbf{h}=-[\kappa_2\sin k_y d,\kappa_1+\kappa_2\cos k_y d]$, so that $\Phi_B=i\int_{-\pi/d}^{\pi/d}\langle\mathbf{u}_\pm|\frac{\partial\mathbf{u}_\pm}{\partial k_y}\rangle dk_y$ retains its same quantized values, that is, $\Phi_{B_\pm}=\pi$ in the nontrivial case, when $\kappa_2>\kappa_1$, while $\Phi_{B_\pm}=0$ for $\kappa_2<\kappa_1$. While a bifurcation occurs above the critical intensity $I>2\varepsilon/g$, creating an additional flat bulk band at frequency $\omega(|k_y|<\sqrt{(Ig/2)^2-\varepsilon^2})=-gI$, this transition does not appear to affect the bulk solitons or the band gap, since it lies outside their frequency range of $[-\varepsilon,\varepsilon]$. Moreover, though localized modes are characterized by their dispersion $\mathscr{P}(\omega)$, which can be related to the local intensity at the edge as $\omega=-gI(y=0)/2$, this cannot be directly compared with the Bloch wave intensity I.

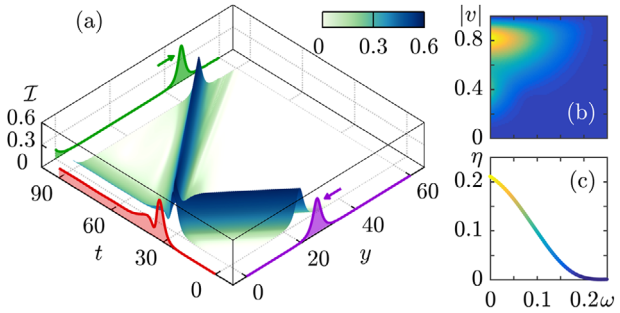

Figure 3. Dynamics in a finite dimer chain. a) Spatiotemporal dynamics in a finite dimer chain with a nontrivial edge at $y=0$. Final and initial snapshots of the intensity distribution are shaded in green and purple, respectively. Here $\kappa=1$, $g=1$, $\varepsilon=0.25$, $\omega=0.075$, $\nu=-0.75$. b) Conversion efficiency to the edge state from an impinging stable soliton $\eta\equiv\mathscr{P}^{(1)}/\mathscr{P}_s$ depending on the soliton frequency and velocity. c) Frequency dependence of the efficiency at fixed $\nu=-0.75$.

This indicates the stationary bulk solitons are more relevant than the bulk nonlinear Bloch waves to the properties of edge states. In particular, edge states emerge at a symmetry-breaking bifurcation of the bulk solitons, which lose their stability. This picture is consistent with recent studies of topological lasers,[32,33] which proposed nonlinear topological transitions protected by particle–hole symmetry. Here the relevant symmetry is inversion symmetry.[34]

Having analyzed the properties of stationary bulk and edge solitons, we now turn to nonlinearity-induced coupling between the two. For this, we consider moving solitons described by Equation (1) with $\nu\neq 0$. They are capable of exciting edge states by reflecting off the topologically nontrivial edge, as illustrated in **Figure 3**. Upon reflection, the conservation of power and energy defines conservation laws for incident and reflected solitons and the excited edge state. The conversion efficiency tends to grow with decreasing frequency of the pump soliton, that is, as the bifurcation point is approached, and for a given soliton frequency there is an optimal velocity maximizing the energy transfer. This effect holds beyond the continuum limit in finite discrete lattices, which is illustrated further in the Supporting Information, where we obtain numerically an optimal conversion efficiency of about 20%.

The model (3) can also be implemented in nonlinear photonic graphene with staggered sublattice potential. For example, we consider an array of waveguides arranged in a honeycomb lattice formed by two sublattices A and B, as shown in Figure 1b.

The tight-binding equations governing the light propagation dynamics read

$$i\partial_t \Psi_{A,j} = M\Psi_{A,j} - \sum_{\langle j,j'\rangle} \Psi_{B,j'}$$
$$i\partial_t \Psi_{B,j} = -M\Psi_{B,j} - \sum_{\langle j,j'\rangle} \Psi_{A,j'} \quad (12)$$

where $\Psi_{A,j}$ and $\Psi_{B,j}$ are the smooth envelopes of the field at the sites A and B of the unit cell j, $\sum_{\langle j,j'\rangle}$ denotes the sum over nearest neighbors, M is a detuning between waveguides A and B controllable by varying the waveguide radii. Performing the Fourier transform $\Psi_{A,B} = \psi_{1,2} e^{-i\omega t + i\mathbf{kr}}$, near the Dirac points of the band gap structure the low-energy Hamiltonian assumes the form

$$\hat{H}_{K_\pm} = \pm\delta k_x \hat{\sigma}_x + \delta k_y \hat{\sigma}_y + M\hat{\sigma}_z \quad (13)$$

Neglecting inter-valley scattering, we restrict our consideration to a single Dirac point. A *valley-Hall domain wall* is created between two insulators characterized by distinct values of the mass, $M(y > 0) = M_0$ and $M(y < 0) = -M_0$. For propagating waves $\propto e^{-i\omega t + ikx}$ bound to the interface $y = 0$, the boundary condition $\psi_1(0) = \mp\psi_2(0)$ holds for $M_0 > 0$ and $M_0 < 0$, respectively.[35] Near the Dirac points, the valley edge states have linear dispersion $\omega = \mp k$ traversing the gap between the hyperbolic cones of bulk states $\omega^2 = k^2 + M_0^2$. Introducing Kerr nonlinearity, using the soliton solution (1) we derive the edge states' nonlinear dispersion

$$\omega = \Delta\omega_{NL} \mp k\,, \quad \Delta\omega_{NL} = -\frac{g}{2}\rho_s\left(\alpha_s = \pm\frac{\pi}{4}\right) \quad (14)$$

which undergoes a shift in the band gap $[-M_0, M_0]$. The valley Chern number formally stays the same as its linear counterpart until the upper band of nonlinear Bloch waves forms a self-crossing loop at above-threshold bulk intensities $I \geq 2M_0$.[36] Thereby, nonlinearity grants control over the frequency and transverse structure of the edge state as defined by $\rho_s(\alpha_s)$. We stress that our solution describes the localization transverse to the edge assuming plane-wave-like profiles with fixed k parallel to the edge. For finite wavepackets, higher order terms in k will induce diffraction along the edge, with weak nonlinearity inducing edge solitons[23] and modulational instability.[14,15]

In contrast to the 1D case, 2D bulk solitons at $M \neq 0$ cannot be obtained analytically. Nevertheless, by analogy with the above results we can consider excitation of valley edge sites by scattering of bulk solitons. Stationary bulk semi-vortex solitons with harmonic time dependence and radial symmetry, whose spinor in the polar coordinate system (r, φ) is given by $[\Psi_1, \Psi_2] = [u(r), iv(r)e^{i\varphi}]e^{-i\omega t}$ at $M_0 > 0$ and $[\Psi_1, \Psi_2] = [-v(r)e^{-i\varphi}, iu(r)]e^{-i\omega t}$ at $M_0 < 0$, are numerically calculated by the shooting method using Chebyshev discretization of the radial coordinate.[28,37] At $M_0 = 1$, solitons are found to be stable for $\omega > 0.388$ in agreement with refs. [38,39]. Propagation dynamics are modeled with a custom numerical code employing a split-step scheme and the Fourier spectral method accomplished by means of the fast Fourier transform. Periodic boundary conditions are applied to the rectangular calculation domain with an equispaced grid. In **Figure 4**a, a topological cavity is created by mass inversion in a circular domain. A clock-wise pulse of edge waves is excited at a closed contour of the cavity by a bulk soliton. The soliton excites persistent topological current and goes away tilted in the opposite direction. In Figure 4b, a soliton initially launched in the y direction is trapped in a waveguide made of two parallel topological interfaces supporting counter-propagating valley edge states. The soliton moves in a zigzag between the waveguide boundaries. Upon each reflection from the the walls, it emits a pulse of edge waves.

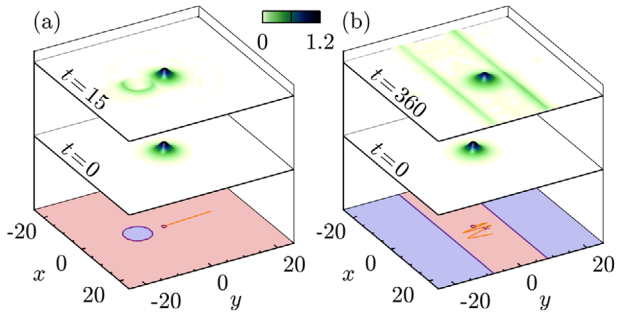

Figure 4. Solitons excite edge states at domain walls created by mass inversion in a 2D Dirac model. Bottom slices show mass maps of a) a circular cavity, and b) two straight interfaces, with domains of positive (reddish) and negative (bluish) masses. Parameters $M_0 = 1$, $g = 1$, $\omega = 0.7$. Middle and top slices: intensity distribution $(|\psi_1|^2 + |\psi_2|^2)^{\frac{1}{2}}$ at the initial and given moment. Locations of the intensity maxima are marked with a dot ($t = 0$) and cross ($t = 360$). The orange straight line and zigzag-like curve visualize trajectories of the soliton center of mass at time intervals of 250 and 500, respectively.

Given the potential to explore the interplay between nonlinear and topological effects in various photonic settings, including where the infinite-contrast tight-binding approximation is inapplicable, the perspective of continuum nonlinear edge models and bifurcation analysis offers valuable insights. Our method can be applied to other classes of topological lattices, with the example of the nonlinear distorted Kagome lattice given in Supporting Information.

In summary, we have studied topological localized states in the nonlinear Dirac model and demonstrated close connections between edge states and self-trapped solitons in topological band gaps. Both can be inferred from phase portraits of the same nonlinear mapping. The bulk solitons resemble the Wannier functions in the linear limit, with nonlinear edge states emerging precisely when the bulk solitons are cut by the edge. This bifurcation of edge states is accompanied by the bulk soliton destabilizing. We furthermore demonstrated numerically that mutual transformations between edge and bulk states, forbidden in linear limit, can occur in the nonlinear regime in 1D and 2D systems. Our findings could have important implications for further developments of nonlinear topological systems not being limited to photonics but spanning through the fields of metamaterials to cold atoms in optical lattices.

Supporting Information

Supporting Information is available from the Wiley Online Library or from the author.

Acknowledgements

This work was supported by the Australian Research Council (Grant DE190100430), the Strategic Fund of the Australian National University, the Russian Foundation for Basic Research (Grants 18-02-00381, 19-52-12053) and the Institute for Basic Science in Korea (IBS-R024-Y1). [Correction added after publication, 28 November 2019: Figure 1 was corrected because of an error in the lower part of panel (b)]

Conflict of Interest

The authors declare no conflict of interest.

Keywords

gap soliton, kerr nonlinearity, nonlinear dynamics, optical lattice, topological edge state, topological photonics

Received: July 4, 2019
Revised: August 17, 2019
Published online: November 4, 2019

[1] L. Lu, J. D. Joannopoulos, M. Soljačić, *Nat. Phys.* **2016**, *12*, 626.
[2] T. Ozawa, H. M. Price, A. Amo, N. Goldman, M. Hafezi, L. Lu, M. C. Rechtsman, D. Schuster, J. Simon, O. Zilberberg, I. Carusotto, *Rev. Mod. Phys.* **2019**, *91*, 015006.
[3] X. Zhou, Y. Wang, D. Leykam, Y. D. Chong, *New J. Phys.* **2017**, *19*, 095002.
[4] Y. V. Kartashov, D. V. Skryabin, *Phys. Rev. Lett.* **2017**, *119*, 253904.
[5] M. A. Bandres, S. Wittek, G. Harari, M. Parto, J. Ren, M. Segev, D. N. Christodoulides, M. Khajavikhan, *Science* **2018**, *359*, eaar4005.
[6] W. Chen, D. Leykam, Y. Chong, L. Yang, *MRS Bull.* **2018**, *43*, 443.
[7] S. Mittal, E. A. Goldschmidt, M. Hafezi, *Nature* **2018**, *561*, 502.
[8] S. Kruk, A. Poddubny, D. Smirnova, L. Wang, A. Slobozhanyuk, A. Shorokhov, I. Kravchenko, B. Luther-Davies, Y. Kivshar, *Nat. Nanotechnol.* **2018**, *14*, 126.
[9] D. Leykam, S. Mittal, M. Hafezi, Y. D. Chong, *Phys. Rev. Lett.* **2018**, *121*, 023901.
[10] S. Wang, L.-J. Lang, L. C. H., B. Zhang, Y. D. Chong, *Nat. Commun.* **2019**, *10*, 1102.
[11] D. Smirnova, S. Kruk, D. Leykam, E. Melik-Gaykazyan, D.-Y. Choi, Y. Kivshar, *Phys. Rev. Lett.* **2019**, *123*, 103901.
[12] V. Peano, M. Houde, F. Marquardt, A. A. Clerk, *Phys. Rev. X* **2016**, *6*, 041026.
[13] O. Bleu, D. D. Solnyshkov, G. Malpuech, *Phys. Rev. B* **2016**, *93*, 085438.
[14] Y. Lumer, M. C. Rechtsman, Y. Plotnik, M. Segev, *Phys. Rev. A* **2016**, *94*, 021801.
[15] Y. V. Kartashov, D. V. Skryabin, *Optica* **2016**, *3*, 1228.
[16] D. Solnyshkov, O. Bleu, B. Teklu, G. Malpuech, *Phys. Rev. Lett.* **2017**, *118*, 023901.
[17] D. R. Gulevich, D. Yudin, D. V. Skryabin, I. V. Iorsh, I. A. Shelykh, *Sci. Rep.* **2017**, *7*, 1780.
[18] C. Li, F. Ye, X. Chen, Y. V. Kartashov, A. Ferrando, L. Torner, D. V. Skryabin, *Phys. Rev. B* **2018**, *97*, 081103.
[19] C.-E. Bardyn, T. Karzig, G. Refael, T. C. H. Liew, *Phys. Rev. B* **2016**, *93*, 020502.
[20] Y. Lumer, Y. Plotnik, M. C. Rechtsman, M. Segev, *Phys. Rev. Lett.* **2013**, *111*, 243905.
[21] D. Leykam, Y. D. Chong, *Phys. Rev. Lett.* **2016**, *117*, 143901.
[22] C. Guan, J. Shi, J. Liu, H. Liu, P. Li, W. Ye, S. Zhang, *Laser Photon. Rev.* **2018**, *13*, 1800242.
[23] M. J. Ablowitz, C. W. Curtis, Y.-P. Ma, *Phys. Rev. A* **2014**, *90*, 023813.
[24] Y. Gerasimenko, B. Tarasinski, C. W. J. Beenakker, *Phys. Rev. A* **2016**, *93*, 022329.
[25] Y. Hadad, A. B. Khanikaev, A. Alù, *Phys. Rev. B* **2016**, *93*, 155112.
[26] Y. Hadad, V. Vitelli, A. Alu, *ACS Photonics* **2017**, *4*, 1974.
[27] Y. Hadad, J. C. Soric, A. B. Khanikaev, A. Alù, *Nat. Electron.* **2018**, *1*, 178.
[28] A. N. Poddubny, D. A. Smirnova, *Phys. Rev. A* **2018**, *98*, 013827.
[29] A. Bisianov, M. Kremer, A. Szameit, U. Peschel, in *Conference on Lasers and Electro-Optics*. Optical Society of America, Washington, DC **2018**, paper FM1E.1.
[30] D. A. Dobrykh, A. V. Yulin, A. P. Slobozhanyuk, A. N. Poddubny, Y. S. Kivshar, *Phys. Rev. Lett.* **2018**, *121*, 163901.
[31] J. Liu, L. B. Fu, *Phys. Rev. A* **2010**, *81*, 052112.
[32] S. Malzard, E. Cancellieri, H. Schomerus, *Opt. Express* **2018**, *26*, 22506.
[33] E. Cancellieri, H. Schomerus, *Phys. Rev. A* **2019**, *99*, 033801.
[34] F. Grusdt, M. Höning, M. Fleischhauer, *Phys. Rev. Lett.* **2013**, *110*, 260405.
[35] X. Ni, D. Smirnova, A. Poddubny, D. Leykam, Y. Chong, A. B. Khanikaev, *Phys. Rev. B* **2018**, *98*, 165129.
[36] R. W. Bomantara, W. Zhao, L. Zhou, J. Gong, *Phys. Rev. B* **2017**, *96*, 121406.
[37] J. Cuevas-Maraver, P. G. Kevrekidis, A. Saxena, A. Comech, R. Lan, *Phys. Rev. Lett.* **2016**, *116*, 214101.
[38] J. Cuevas-Maraver, P. G. Kevrekidis, A. B. Aceves, A. Saxena, *J. Phys. A* **2017**, *50*, 495207.
[39] H. Sakaguchi, B. A. Malomed, *Phys. Rev. A* **2018**, *97*, 013607.